

Efficient acceleration of electrons with counterpropagating intense laser pulses in vacuum and underdense plasma

Zheng-Ming Sheng,¹ Kunioki Mima,² Jie Zhang,¹ and Jürgen Meyer-ter-Vehn³¹Laboratory of Optical Physics, Institute of Physics, Chinese Academy of Sciences, Beijing 100080, China²Institute of Laser Engineering, Osaka University, Suita, Osaka 565-0871, Japan³Max-Planck-Institut für Quantenoptik, D-85748 Garching, Germany

(Received 8 April 2003; published 29 January 2004)

We propose that efficient acceleration of electrons in vacuum and underdense plasmas by an intense laser pulse can be triggered in the presence of another counterpropagating or intersecting laser pulse. This mechanism works when the laser fields exceed some threshold amplitudes for stochastic motion of electrons, as found in single-electron dynamics. Particle-in-cell simulations confirm that electron heating and acceleration in the case with two counterpropagating laser pulses can be much more efficient than with one laser pulse only. Two different diagnoses show that the increased heating and acceleration are caused mainly by direct laser acceleration rather than by plasma waves. In plasma at moderate densities such as a few percent of the critical density and when the underdense plasma region is large enough, the Raman backscattered and side-scattered waves can grow to a sufficiently high level to serve as the second counterpropagating or intersecting pulse and trigger the electron stochastic motion. As a result, even with a single intense laser pulse only in plasma, electrons can be accelerated to an energy level much higher than the corresponding laser ponderomotive potential.

DOI: 10.1103/PhysRevE.69.016407

PACS number(s): 52.38.Kd, 52.35.Mw, 52.50.Jm

I. INTRODUCTION

The mechanisms leading to significant acceleration of electrons in laser-plasma interactions have been the topic of many theoretical and experimental studies over the past two decades. With the development of tabletop ultraintense lasers, ways of converting the ultrahigh-density laser energy into particle beams have been attracting renewed attention due to their potential applications [1–3]. These include the fast ignition of ICF targets by high current multi-MeV electron beams [4,5], generation of collimated energetic ion beams through electron heating and acceleration [6], compact x-ray and γ -ray source for laser-driven radiography, laser-driven nuclear processes [1,3,7,8], and compact and low-costed laser wake-field accelerators, etc. [9–13]. A few mechanisms of laser-driven electron acceleration have been proposed, including plasma-wave acceleration [9–13], direct laser acceleration with the assistance of additional fields or by the laser ponderomotive force [14–18], and mixed acceleration from both the transverse and longitudinal fields [19,20]. The first two mechanisms usually occur in laser interaction with underdense plasmas, while the third case usually finds in laser interaction with overdense plasmas.

This work is devoted to an extended investigation of a kind of direct laser acceleration of electrons, i.e., the stochastic heating and acceleration of electrons in counterpropagating intense laser fields [17]. It was found earlier from particle-in-cell (PIC) simulations that, when an intense laser pulse with a slowly rising front propagates in underdense plasma, electrons can be accelerated significantly far beyond the ponderomotive potential level of the incident pulse. Meanwhile, the excited plasma wave remains at a very high level. Further studies reveal the presence of the betatron resonance acceleration mechanism [16], which works most

effectively when a self-focusing channel is formed. On the other hand, two of us find that very efficient acceleration by the intense laser pulse also occurs in the presence of a *transverse* stochastic field [15]. The oscillation energy of electrons inside the laser pulse can be unlocked by the stochastic perturbations. The essential role of the perturbations is not to heat the electrons directly, but to dephase the electrons and thereby to allow for net energy transfer. In that work, the transverse stochastic field is left as a free parameter. Until recently we found that the Raman backscattered wave can serve as the transverse stochastic field [17]. Moreover, we find that another counterpropagating laser field with a relatively small amplitude can play a similar role as the stochastic perturbations in dephasing the electrons.

In the similar interaction configuration, one notes that the excitation of periodic accelerating structures has also been found with counterpropagating laser pulses in underdense plasma [21]. It is associated with the *coherent motion* of electrons driving by the two colliding laser pulses slightly detuned by the electron plasma frequency. Here, in contrast, our mechanism of electron acceleration is associated with the *stochastic motion* of electrons, which occurs when the amplitudes of two laser pulses exceed some thresholds, now easily accessible with current ultrashort laser pulses employing the chirped pulse amplification technology. Moreover, the present mechanism is insensitive to their frequency differences of the two laser pulses. In plasma at a few percent of the critical density, the Raman backscattering wave of the driving pulse can serve as the counterpropagating laser pulse, which could be intense enough to trigger stochastic acceleration if the driving pulse has an intensity over $I\lambda^2 \sim 10^{18} \text{ W cm}^{-2} \mu\text{m}^2$. Stochastic heating could be responsible for the hot electron generation observed in PIC simulations by Adam *et al.* [22], where it is found that the hot electron generation is closely associated with parametric in-

stabilities. Stochastic heating of electrons in a standing wave formed by incoming and reflected waves in front of a solid target has been suggested [23]. Therefore the present mechanism works widely in relativistic-intense laser interaction with underdense plasma. It may also help to explain how the maximum electron energy can exceed the dephasing limit for particle acceleration from plasma wave breaking observed in some PIC simulations [24]. Experimental evidence of stochastic heating has been revealed recently with the use of two crossed laser pulses [25].

The paper is organized as follows. Starting with the single-electron dynamics calculation in Sec. II, we calculate the electron trajectory in momentum phase space in two counterpropagating or intersecting plane electromagnetic waves. We calculate the Liapunov exponent to examine if there exists stochastic motion, from which we obtain the threshold amplitudes for stochastic motion. In Sec. III, we present particle-in-cell simulation results to show how electrons can be accelerated much more efficiently with the presence of a counterpropagating pulse than without it. Using different diagnoses such as the angular directions of electrons and separating energy gain or loss due to the transverse field from that due to the longitudinal field, we confirm that electron acceleration observed in the simulations is caused by the laser fields rather than by plasma waves. Two-dimensional effects are also discussed. A summary is given in Sec. IV.

II. SINGLE-ELECTRON DYNAMICS IN VACUUM

It is well known that the motion of single electrons in a plane electromagnetic wave is integrable [26], and the maximum kinetic energy of electrons is determined following the initial conditions. However, if there is a perturbation to electron motion in the plane wave, such as another plane wave [27–29], a static electric or magnetic field [14], or a random perturbation [15], the corresponding Hamiltonian is usually not integrable. In general, stochastic electron motion sets in when certain thresholds of the wave amplitudes are exceeded [30]. In this case, the maximum kinetic energy of electrons is not determined, and acceleration of electrons to much higher energy than in a single plane wave is possible. There have been considerable studies on electron motion in multiwave systems [14,27–30]. Based upon the single particle dynamics, it has been proposed by Mendonca and Doveil that the formation of suprathermal electron tails observed in laser plasma interaction may be explained by the occurrence of stochastic motion of electron in two electromagnetic (em) waves [29,31]. However, this and other earlier studies on electron motion in a standing longitudinal plasma wave or two electromagnetic waves have been limited to the problem of the stochastic instability near the separatrices, and mostly in nonrelativistic electron motion. The potential of this stochastic instability in particle acceleration in plasma with powerful lasers focused up to relativistic intensities has not been fully explored before.

We start by considering the electron motion in two colliding planar laser fields in vacuum. The laser pulses can be described by their vector potential $\mathbf{A}_i = a_i(\xi_i)\cos(\xi_i)\hat{\mathbf{y}} \equiv A_i\hat{\mathbf{y}}$,

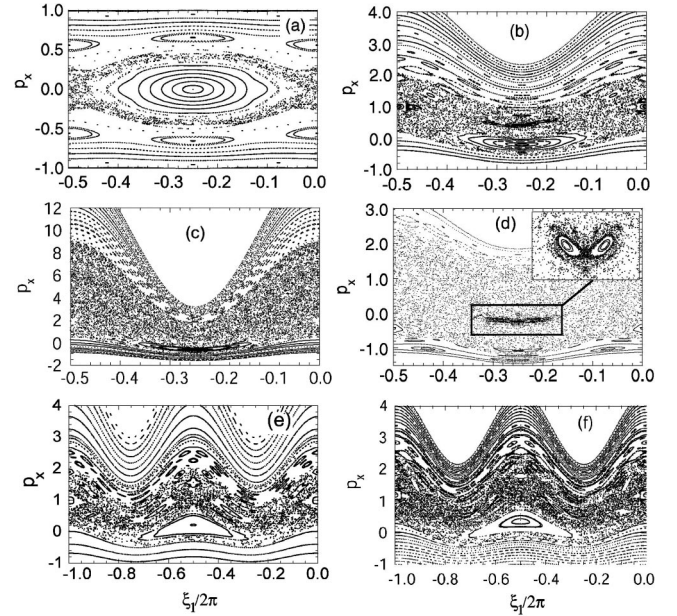


FIG. 1. Surface of section plots at $\xi_2 - \xi_1 = 2N\pi$ [for frames (a)–(d)] or $\xi_2 = 2N\pi$ [for frames (e) and (f)] for electron motion in counterpropagating laser fields. (a) $a_1 = a_2 = 0.3$ and $\omega_1 = \omega_2$; (b) $a_1 = 1.0$, $a_2 = 0.1$, and $\omega_1 = \omega_2$; (c) $a_1 = 2.0$, $a_2 = 0.1$, and $\omega_1 = \omega_2$; (d) $a_1 = 1.0$, $a_2 = 0.42$, and $\omega_1 = \omega_2$; (e) $a_1 = 1.0$, $a_2 = 0.1$, and $\omega_1 = \omega_2$; (f) $a_1 = 1.0$, $a_2 = 0.1$, $\omega_2 = 0.8\omega_1$.

where $i = 1, 2$, $\xi_1 = x - t + \psi_1$, and $\xi_2 = k_2(x + t) + \psi_2$, the frequencies of the two laser pulses are ω_1 and ω_2 , respectively, x and t are normalized to c/ω_1 and ω_1^{-1} , respectively, $k_2 (= \omega_2/c)$ and ω_2 are normalized to ω_1/c and ω_1 , respectively, and ψ_1 and ψ_2 are constants. The first pulse propagates in positive x direction and the second one propagates in negative x direction. The Hamiltonian for electrons is given by

$$H = [1 + (\mathbf{P} + \mathbf{A})^2]^{1/2}, \quad (1)$$

where the canonical momentum $\mathbf{P} = \mathbf{p} - \mathbf{A}$ is normalized by mc and vector potential \mathbf{A} by mc^2/e . Since \mathbf{A} is independent of y , one finds that $P_y = \text{constant} = p_{y0}$. For simplicity, we assume $p_z = 0$ in the following. Therefore the longitudinal motion can be described by Hamiltonian $H = [1 + p_x^2 + (p_{y0} + A_1 + A_2)^2]^{1/2}$. This Hamiltonian is still more complicated than that for electron motion in counterpropagating plasma waves [27]. Even in the nonrelativistic limit, making the canonical transform with $\eta = x - t$, $F_2 = \eta p_\eta$, and $p_\eta = p_x$, assuming $p_{y0} = 0$ and $\epsilon = a_2/a_1 \ll 1$, the resulting Hamiltonian contains two perturbation terms oscillating at different frequencies.

A. Surface of section plots

The instability regime for stochastic motion can be examined in geometry by use of surface of section plots. Figure 1 shows the surface of section plots at $\xi_2 - \xi_1 = 2N\pi$ or $\xi_2 = 2N\pi$ for two lasers at various amplitudes, where N is an integer. When the two laser pulses are at the same frequency,

the Hamiltonian is a periodic function of ξ_1 at a period of π on the surface of section at $\xi_2 - \xi_1 = 2N\pi$. When the amplitudes of the two pulses are the same, the electron trajectories in longitudinal momentum space are symmetric about zero as shown in Fig. 1(a). Electron trapping is found around $(p_x, \xi_1) = (0, -(2N+1)\pi/2)$ by the ponderomotive potential resulting from the beating of the two laser pulses. Stochastic motion first appears around the separatrices. According to the Kolmogorov-Arnold-Moser (KAM) theorem [30], there exist many KAM tori around a separatrix. Local stochastic motion sets in when nearby KAM tori overlap [32]. Thresholds for local stochastic motion have been estimated to be about $a_1 a_2 = 1/16$ by Mendonca [29]. When the amplitude of the forward-moving pulse a_1 is larger than a_2 for the backward-moving pulse, the electron trajectories become nonsymmetric about zero; stochastic motion of electrons spreads widely in positive momentum space. The larger the amplitude a_1 , the wider the region for stochastic motion in positive momentum space, as shown in Figs. 1(b)–1(c). For a given a_2 , the width for stochastic motion scales roughly proportional to a_1^2 . One notes that there remains regular motion for electrons trapped around $(p_x, \xi_1) = (0, 0)$, where acceleration cannot occur. However, with the increase of a_1 or a_2 further, this trapping island is gradually suppressed. Before it is fully suppressed, bifurcation occurs at certain amplitudes when the primary trapping island splits into two parts as shown in Fig. 1(d). This shows a transition of the stochastic motion from a local to a global one, where, in the latter case, electrons initially at rest or with small energy will be driven into stochastic motion and gain energy from laser fields. We have checked the surface of section plots on the surface $\xi_2 = 2N\pi$, which show similar features as stated above, except for that the corresponding Hamiltonian changes with ξ_1 at a period of 2π . Figure 1(e) shows an example of the section plots on the surface $\xi_2 = 2N\pi$. Up to now, we have taken the frequencies of the two pulses to be the same. If the frequency of the second pulse is changed, the basic features about the stochastic character are qualitatively similar, as shown in Fig. 1(f), for an example. This indicates that the stochastic motion is not sensitive to the frequency difference of the two pulses.

Figure 2 shows the trajectories of a test electron in momentum phase in vacuum with a single infinite plane em wave A_1 or two counterpropagating plane em waves $A_1 + A_2$. In a single em wave, the momentum of the electron is determined by [2,26] $p_y + A_1 = C_1$ and $\gamma - p_x = C_2$, where C_1 and C_2 are constants. If $C_1 = 0$ and $C_2 = \sqrt{1 + a_1^2/2}$, then one finds the solution with zero average drifting velocity given by

$$p_y = -A_1, \quad p_x = \frac{p_y^2 - a_1^2/2}{2\sqrt{1 + a_1^2/2}}, \quad (2)$$

where a_1 is the amplitude of pulse A_1 . Figure 2(a) shows the parabolic line between p_x and p_y as described by Eq. (2). If there is the second counterpropagating wave, the electron trajectory in the momentum space is no longer confined to the parabolic line. Instead, it spreads in the momentum

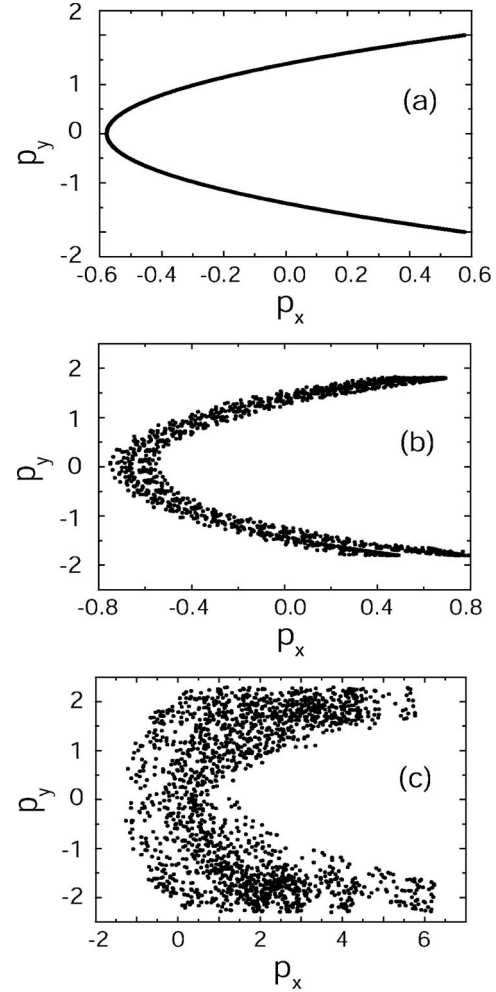


FIG. 2. Electron motion in momentum space in one plane electromagnetic (em) wave or two plane em waves. (a) $a_1=2.0$ and $a_2=0.0$; (b) $a_1=2.0$ and $a_2=0.2$; (c) $a_1=2.0$ and $a_2=0.3$.

space. The larger the amplitude of the second wave, the larger the momentum space and the maximum longitudinal momentum, as illustrated in Figs. 2(b) and 2(c).

B. Threshold amplitudes for stochastic motion

The Liapunov exponents can provide a quantitative measure of the degree of stochasticity for a given Hamiltonian system, which enable us to judge if stochastic motion sets in for a trajectory [30]. Let the test electron initially at rest and the amplitudes of the infinite planar laser pulses increase from zero in a function $\tan(t/t_L)$ with $t_L = 50\tau$ and τ the time of a laser cycle. The Liapunov exponents are calculated when the laser fields reach the peak amplitudes at a_1 and a_2 for $t > 2t_L$. As either the amplitude a_1 or a_2 increases, the Liapunov exponents increase suddenly as the laser amplitudes exceed some threshold amplitudes. Figure 3(a) shows a typical example of the calculated Liapunov exponents for different field amplitudes, which show a sudden increase as a_2 is enhanced to 0.3 while keeping $a_1 = 1.5$. We assume that full stochastic motion occurs when the corresponding Liapunov exponent increases suddenly to exceeding 0.1 as the

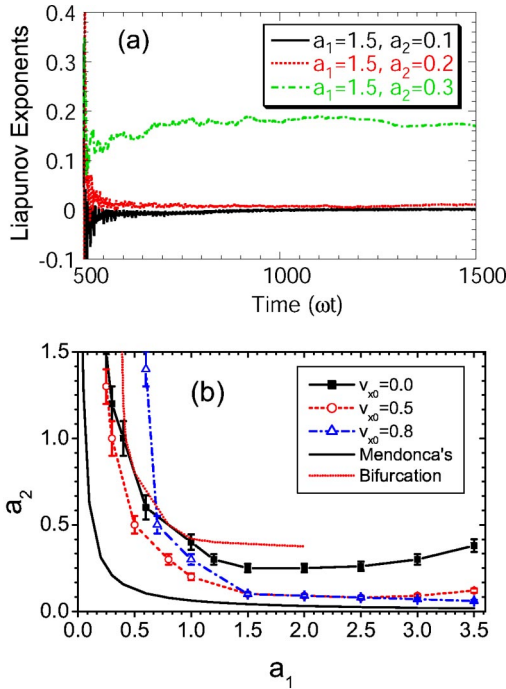


FIG. 3. (a) Liapunov exponents for a test electron moving in counterpropagating laser fields with different incident field amplitudes. (b) Threshold amplitudes for stochastic motion in counterpropagating laser fields obtained numerically for electrons with different initial velocities. Also shown are the thresholds for local stochastic motion by Mendonca and for the occurrence of bifurcation for trajectories trapped in the fundamental island around $(p_x, \xi_1) = (0, 0)$.

field amplitudes increase. Since we start with the test electron at rest initially, the obtained thresholds should be associated with the global stochasticity around the fundamental trapping island in the surface of section plot. This is shown in Fig. 3(b) by the solid line marked with $v_{x0} = 0$. It is approximately $a_1 a_2 \sim 1/2$, which is larger than that estimated by Mendonca for local stochastic motion [29], but close to that for the bifurcation of the primary trapping island. One notes that for $a_1 > 2.0$, the thresholds for a_2 slightly increase with a_1 . This can be attributed to the fact that for a given a_2 , the width of the primary trapping island increases with a_1 , such that the electron motion tends to become regular. If the initial longitudinal momentum of the test electron is nonzero, the threshold amplitudes can either reduce or increase. In particular, if the initial velocity is positive such as driven by the ponderomotive force at the front of the forward-propagating pulse (with amplitude a_1), the threshold amplitude for a_2 reduces significantly for the regime of $a_1 > a_2$, as shown in Fig. 3(b). For $v_{x0} \geq 0.5$, for example, the threshold amplitude of the counterpropagating pulse a_2 reduces to only about 0.1 or less when $a_1 > 1.5$. In addition, we mention that the so-called global stochastic motion is only limited to the region between some upper and lower boundaries in longitudinal momentum, beyond which, the electron motion becomes regular again. For example, if the longitudinal velocity of the test electron is sufficiently larger, its trajectory in

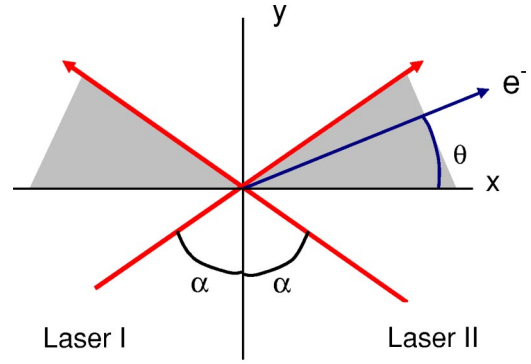


FIG. 4. Schematic plot of electron scattering in two intersecting laser pulses.

the colliding laser fields becomes regular again and further acceleration of the electron is not possible.

C. Electron dynamics in intersecting laser pulses

We consider a geometry shown in Fig. 4, where two laser pulses intersect at an angle 2α and interact with an electron initially located at the coordinate origin. In this case, we have two different cases for the laser pulses, i.e., the case for P -polarized planar pulses if the vector potential is inside the xy plane and that for S -polarized pulses if the vector potential is perpendicular to the xy plane. For the P -polarization case, the vector potential for the planar pulses in vacuum can be written as

$$\mathbf{A}_i = a_i(\xi_i) \cos(\xi_i) (\hat{\mathbf{x}} \cos \alpha \mp \hat{\mathbf{y}} \sin \alpha), \quad i = 1, 2,$$

where $0 \leq \alpha \leq \pi/2$, $\xi_1 = y \cos \alpha + x \sin \alpha - t + \psi_1$, and $\xi_2 = k_2(y \cos \alpha - x \sin \alpha - t) + \psi_2$, x and y are normalized to c/ω_1 , t is normalized to ω_1^{-1} , $k_2 = (\omega_2/c)$ and ω_2 are normalized to ω_1/c and ω_1 , respectively, ψ_1 and ψ_2 are constants; the upper and lower cases in the symbols \mp and \pm appeared above and later correspond to $i = 1$ and 2 , respectively. For the S -polarization case, the vector potentials of the two pulses are simply

$$\mathbf{A}_i = a_i(\xi_i) \cos(\xi_i) \hat{\mathbf{z}}, \quad i = 1, 2.$$

Using the canonical transform $F_2 = (t - y \cos \alpha) P_T$, one finds $P_y = -\cos \alpha P_T$, $T = t - y \cos \alpha$, and the new Hamiltonian: $\bar{H}(P_x, P_T, x, T) = \gamma(P_x, P_T, x, T) + P_T$. Since the new Hamiltonian is independent of time t explicitly in terms of the new variables, one finds

$$P_y - \gamma \cos \alpha = C, \quad (3)$$

where $C = p_{y0} - \gamma_0 \cos \alpha$ is a constant with p_{y0} and γ_0 the initial values of the y component of momentum and the relativistic factor, respectively, $P_y = p_y - A_y \equiv p_y + (A_1 - A_2) \sin \alpha$ for P polarization and $P_y = p_y$ for S polarization. Let $\tan \theta = p_y/p_x$, assuming $p_z = 0$ when the laser pulses propagate away and recalling $\gamma^2 = 1 + p_x^2 + p_y^2$, one finds the angular direction of electrons satisfies

$$\tan(\theta) = \pm \left[\frac{\gamma^2 - 1}{(\gamma \cos \alpha + C)^2} - 1 \right]^{-1/2}. \quad (4)$$

Note that this relation is independent of the laser polarization. It can reduce to different limits as discussed elsewhere [33]. With the integral constant Eq. (3) and another one $P_z = \text{const}$ accounting for that \bar{H} is independent of the coordinate z , one only needs to solve P_x . Therefore it reduces to the same problem of solving the x component of momentum as in the case with counterpropagating laser pulses.

Alternatively, if one transforms all variables into a frame moving with velocity $\mathbf{V}_0 = \hat{\mathbf{y}}c \cos \alpha$, then the two pulses appear as counterpropagating pulses. The four-vector for frequency and wave number in the moving frame are $(\omega'_i, k'_{ix}, k'_{iy}, k'_{iz}) = (\omega_i \sin \alpha, \pm k_0 \sin \alpha, 0, 0)$. For P -polarized laser pulses, the components of the four-vector potential are

$$(\phi'_i, A'_{ix}, A'_{iy}, A'_{iz}) = (\pm A_i \cos \alpha, A_i \cos \alpha, \mp A_i, 0),$$

assuming $\phi = 0$ in the laboratory frame, where $A_i = a_i(\xi'_i) \cos(\xi'_i + \psi_i)$, $\xi'_i = k_i(\pm x' - t') \sin \alpha + \phi_i$. The equation of motion for electrons in the moving frame is

$$\frac{d\mathbf{p}'}{dt'} = \frac{d\mathbf{A}'}{dt'} - \nabla(\mathbf{v}' \cdot \mathbf{A}') + \nabla\phi', \quad (5)$$

where the momentum \mathbf{p}' is normalized to mc , the velocity \mathbf{v}' normalized to c , the vector potential $\mathbf{A}' = \mathbf{A}'_1 + \mathbf{A}'_2$, the scalar potential ϕ' are normalized to mc^2/e , and the first ∇ acts on \mathbf{A}' only. For the P -polarization case, substituting the four-vector potential into Eq. (5), one can find two integral constants of motion from its y and z components:

$$p'_y = p'_{y0} + A_2 - A_1, \quad p'_z = p'_{z0}, \quad (6)$$

where p'_{y0} and p'_{z0} are the initial momentum components of electrons in the moving frame. Note that if transforming p'_y back to the laboratory frame $p'_y = (p_y - \gamma \cos \alpha) / \sin \alpha$ and $p'_{y0} = (p_{y0} - \gamma_0 \cos \alpha) / \sin \alpha$, and substituting them into Eq. (6), we obtain Eqs. (3) and (4) again. The resulting x component of Eq. (5) reduces to

$$\frac{dp'_x}{dt'} = -\frac{1}{2\gamma'} \frac{\partial}{\partial x'} (p'_{y0} + A_2 - A_1)^2, \quad (7)$$

where $\gamma' = (1 + p'^2_x + p'^2_y + p'^2_z)^{1/2}$ with p'_y and p'_z described by Eq. (6).

For the S -polarization case, the corresponding components of the four-vector potential are simply

$$(\phi'_i, A'_{ix}, A'_{iy}, A'_{iz}) = (0, 0, 0, A_i).$$

Substituting them into Eq. (5), one finds two integral constants of motion for its y and z components:

$$p'_y = p'_{y0}, \quad p'_z = p'_{z0} + A_1 + A_2. \quad (8)$$

Again one can obtain Eq. (4) by transforming p'_y and p'_{y0} back to the laboratory frame and substituting them into Eq. (8). The x -component equation takes the form of

$$\frac{dp'_x}{dt'} = -\frac{1}{2\gamma'} \frac{\partial}{\partial x'} (p'_{z0} + A_1 + A_2)^2, \quad (9)$$

where $\gamma' = (1 + p'^2_x + p'^2_y + p'^2_z)^{1/2}$ with p'_y and p'_z described by Eq. (8). Therefore, for both the P - and S -polarization cases, the problem of electron dynamics in intersecting laser pulses reduces to solving the x component of momentum described by Eqs. (7) or (9) as similar to that in counterpropagating laser pulses.

The difference for the electron dynamics between the P - and S -polarization cases can be illustrated by the surface of section plots. Assuming that the two pulses are at the same frequency and electrons are at zero momenta ($p_{y0} = p_{z0} = 0$) in the laboratory frame in the absence of laser field, we find that the right-hand sides of Eqs. (7) and (9) are periodic in terms of ξ'_1 at the surface $\xi'_2 - \xi'_1 = 2N\pi$ for P and S polarization, respectively. The period is 2π for the P -polarization case, while it becomes π for the S -polarization case. Figure 5 shows the surface of section plots in the (p'_x, ξ'_1) plane at $\xi'_2 - \xi'_1 = 2N\pi$ for both the P - and S -polarization cases when the two pulses are at the same frequency. Frames (a)–(d) are for P polarization and frames (e)–(h) are for S polarization. By comparing these plots, one concludes that stochastic motion is more easily triggered for P polarization than for S polarization. Meanwhile, for the same laser amplitudes, the momentum space for stochastic motion is larger for P polarization than for S polarization. When the two pulses are at different frequencies, one can make the surface of section plots at the surface $\xi'_2 = 2N\pi$. The results are qualitatively similar as for two pulses with the same frequency stated above.

In a similar way, we calculate the thresholds of stochastic motion when the two pulses are intersecting with an angle by solving Eqs. (7) and (9). Figures 6(a) and 6(b) show the threshold amplitudes for a test electron initially at rest, where two pulses intersecting at angles of $2\alpha = 60^\circ$ and 90° , respectively. Obviously, they depend upon the intersecting angles. Moreover, for both cases they are found to be larger than that given in Fig. 3(b) for the case with counterpropagating pulses $2\alpha = 180^\circ$. The threshold amplitudes tend to increase with the decrease of the intersecting angle. In particular, when $\alpha = 0^\circ$, i.e., two pulses copropagate, there is no stochastic electron motion for two pulses at arbitrary amplitudes since the corresponding Hamiltonian becomes integrable. Figure 6 also indicates that the threshold amplitudes for S -polarized intersecting pulses are slightly larger than for P -polarized pulses.

III. ELECTRON HEATING AND ACCELERATION IN PLASMA

A. One-dimensional particle-in-cell simulations

To confirm this acceleration mechanism, we have performed numerical simulations with PIC codes. We first try to

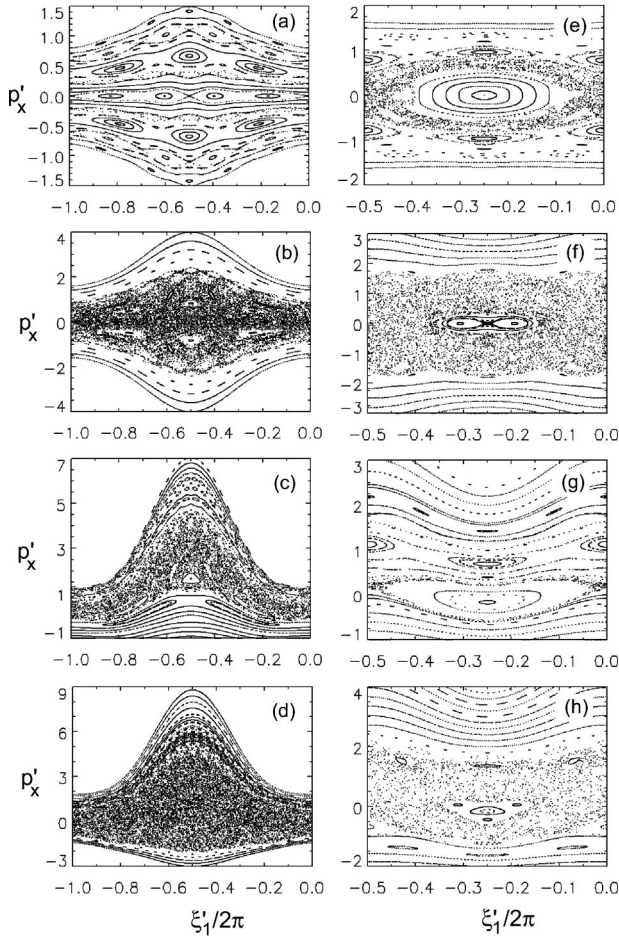


FIG. 5. Surface of section plots at $\xi_2 - \xi_1 = 2N\pi$ for electron motion in intersecting laser fields either *P* or *S* polarized at intersecting angle $2\alpha = 90^\circ$. (a) $a_1 = a_2 = 0.3$ for *P* polarization; (b) $a_1 = a_2 = 0.5$ for *P* polarization; (c) $a_1 = 1.0$ and $a_2 = 0.1$ for *P* polarization; (d) $a_1 = 1.0$ and $a_2 = 0.5$ for *P* polarization; (e) $a_1 = a_2 = 0.5$ for *S* polarization; (f) $a_1 = a_2 = 0.9$ for *S* polarization; (g) $a_1 = 1.0$ and $a_2 = 0.1$ for *S* polarization; (h) $a_1 = 1.0$ and $a_2 = 0.5$ for *S* polarization.

simulate it with a one-dimensional (1D) PIC code since it is essentially a one-dimensional effect. In simulations, the plasma slab is homogeneous, which occupies a region of $L = 50\lambda - 200\lambda$, where λ is the incident laser wavelength. We leave enough vacuum space on both sides of the plasma slab. The laser pulses, which are semi-infinite and at the same frequency, increase to the maximum amplitudes in 50 laser cycles. We have divided the simulation box into 50 or 100 cells/wavelength to ensure a high accuracy in the numerical integration.

We first set the electron density $n = 0$ in the PIC simulations. In this case, there is not any induced electrostatic field in the simulation box, and the laser pulses are actually interacting with many test electrons distributed homogeneously in vacuum. Figure 7(a) shows the electron energy distributions obtained using a semi-infinite pulse with a peak amplitude $a_1 = 3.0$ and without or with the second counterpropagating pulse at an amplitude $a_2 = 0.1$. In the case of without the second pulse, electrons can only be accelerated to the maxi-

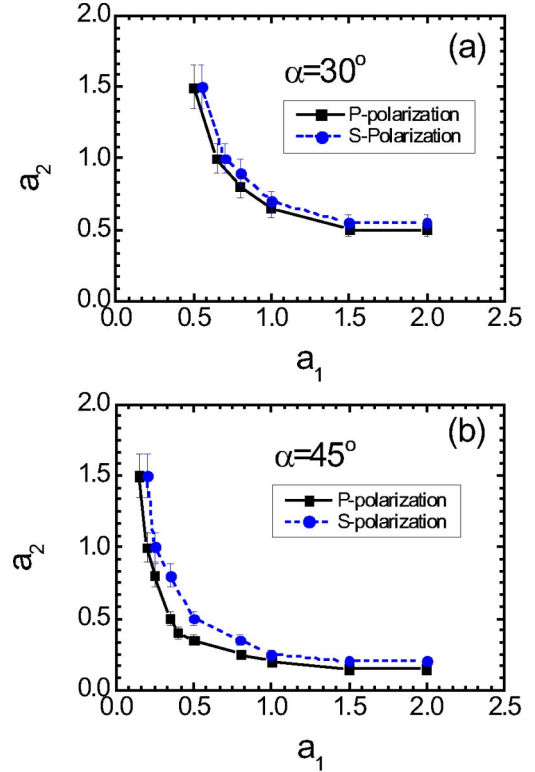


FIG. 6. Threshold amplitudes for stochastic motion when a test electron moves in the two intersecting laser fields. (a) For the intersecting angle $2\alpha = 60^\circ$; (b) for the intersecting angle $2\alpha = 90^\circ$.

imum energy $\gamma - 1 = a_1^2/2$ when electrons are with zero initial velocity [15], which is $\gamma - 1 = 4.5$ for $a_1 = 3.0$. However, if there is the second pulse, the maximum kinetic energy can be more than three times that without it. This can only be attributed to the stochastic acceleration since there is no other field except for the laser fields. Meanwhile, the amplitudes of the two pulses already exceed the thresholds for stochastic electron motion as shown in Fig. 3(b) [see the curve for $v_{x0} = 0.8$]. This is due to the fact that the ponderomotive force of the first pulse preaccelerate electrons to a longitudinal velocity $p_x/\gamma = a_1^2/(2 + a_1^2) = 0.82$, so that the amplitude of the second pulse can be as small as 0.1 for the occurrence of stochastic motion. We find that the temperature tends to be saturated after interaction for a certain period of time. This can be explained partially by surface of section plots, which shows that stochastic motion is found only in limited phase space around the separatrices. For very energetic electrons, their trajectories remain regular, and therefore net energy gain from the laser fields does not occur. This simple example demonstrates obviously that the second counterpropagating pulse can trigger the stochastic motion, which leads to effective energy transfer from laser fields to electrons.

Figure 7(b) shows the case when the laser pulses interact with a plasma slab at the density $n = 0.01n_c$ (n_c is the critical density). Similar to the previous case in vacuum, both the electron temperatures and maximum electron energy are much higher in the presence of the second pulse, even though it is only with an amplitude $a_2 = 0.1$. Note that the peaks near $\gamma - 1 = 3$ in the distributions are due to the pon-

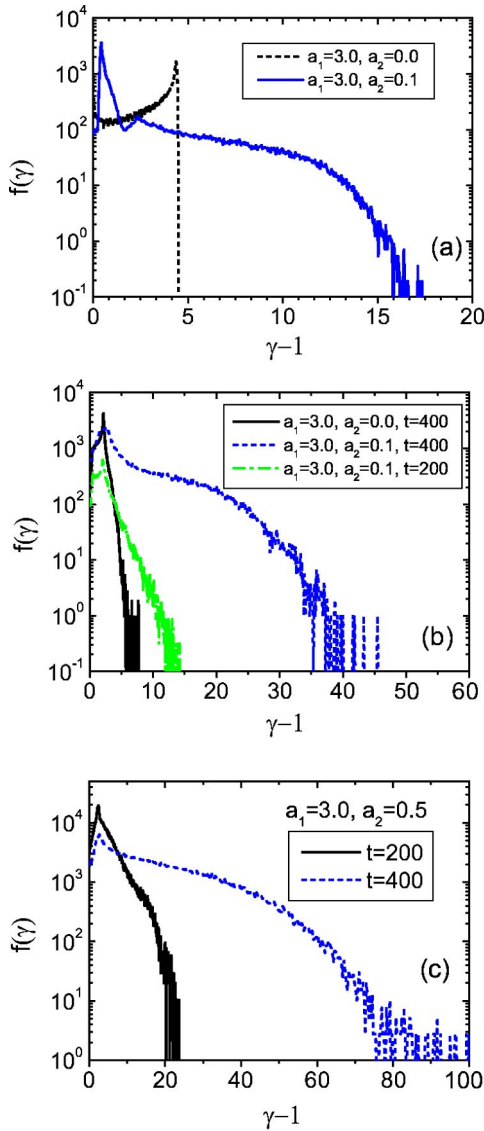


FIG. 7. Electron energy distributions (not normalized) from 1D PIC simulations of laser interaction with test electrons in vacuum or a plasma slab at a density $n=0.01n_c$ and with a thickness of $L=50\lambda$. (a) With test electrons in vacuum at $t=400\tau$; (b) with the plasma slab at $t=400\tau$; (c) with the same plasma slab but at different laser fields at $t=200\tau$ and 400τ . The incident laser pulses are semi-infinite and their fronts meet at $t=100\tau$.

deromotive push with semi-infinite pulses, which would be absent for pulses with finite duration. In comparison with Fig. 7(a), for the same counterpropagating laser pulses, electrons are accelerated to a higher temperature in plasma than in vacuum. This is related to the induced strong electrostatic fields near the plasma-vacuum boundaries, which tend to draw these accelerated electrons outside the plasma slab back, and then they are further accelerated by the laser fields to other stochastic regimes with high initial energies. This may also be attributed to the electron acceleration in the presence of an arbitrary stochastic field, where there is no upper limit for the maximum electron energy [15]. Here this stochastic field can be considered as a combination of the second pulse and the induced electrostatic field. In addition,

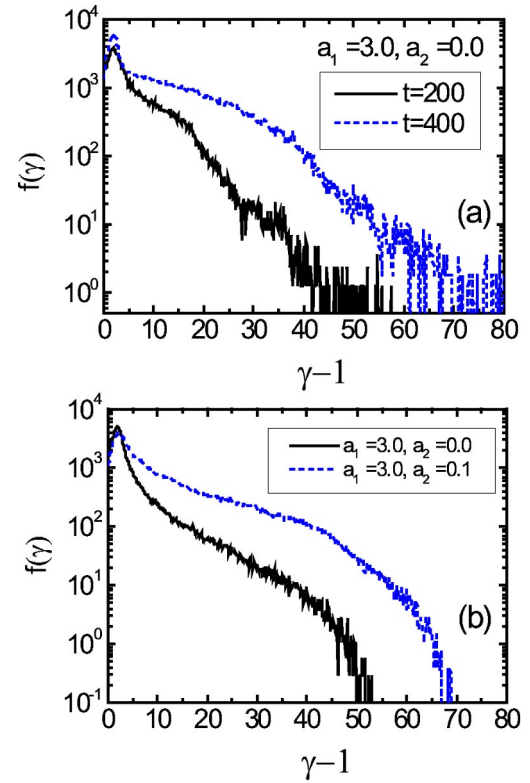


FIG. 8. Electron energy distributions (not normalized) from 1D PIC simulations. (a) The plasma slab is with a thickness of $L=50\lambda$ but with an increased density at $n=0.04n_c$. A semi-infinite laser pulse is incident with a peak amplitude $a_1=3.0$; (b) the plasma slab is with a thickness of $L=200\lambda$ and with a density at $n=0.01n_c$. Shown are the distributions at $t=600\tau$.

if one increases the amplitude of the second pulse, the corresponding electron temperature is also enhanced within in the same time duration, as shown in Fig. 7(c), for example. In passing, we mention that if we change the initial phases of the incident laser pulses, the electron energy distributions can be changed. This is most obvious for the relatively low energy part in the energy distributions. However, the high energy tail appears to be not very sensitive to the initial phase differences of the laser pulses.

B. Effects of the density and length of the plasma slab

If fixing the length of the plasma slab, but increasing the plasma density, one finds that electron can be significantly accelerated to well beyond the ponderomotive potential level, even if one uses a single laser pulse only. Figure 8(a) displays electron energy distributions when the initial plasma density is increased to $n=0.04n_c$ while retaining its length $L=50\lambda$ and the pulse amplitude $a_1=3.0$ as in Fig. 7(b). It shows that the highest electron energy is larger than the ponderomotive potential by over one order of magnitude. Alternatively, if one fixes the plasma density, but increases the length of the plasma slab, we also find significant acceleration of electrons with a single laser pulse. In Fig. 8(b), we plot energy distributions when the plasma length is increased to $L=200\lambda$ while retaining the plasma density $n=0.01n_c$.

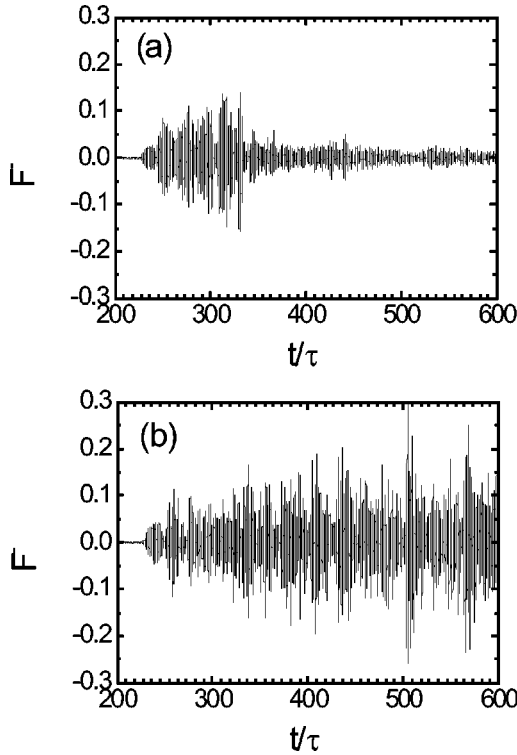


FIG. 9. Raman backscattered light from 1D PIC simulations when a semi-infinite laser pulse with peak amplitude $a_1 = 3.0$ is incident onto a plasma slab with a density $n = 0.01n_c$. (a) The plasma slab is with a thickness of $L = 50\lambda$; (b) the plasma slab is with a thickness of $L = 200\lambda$.

and the pulse amplitude $a_1 = 3.0$. In these two examples, the electron acceleration is closely associated with the excitation of Raman backscattered waves [22,34–37], which achieve amplitudes even higher than 0.1 and trigger the stochastic acceleration.

To illustrate more clearly the effects of the plasma density and length, we plot the Raman backscattered waves in Figs. 9(a) and 9(b) for plasma slabs at the same density $n = 0.01n_c$ but with different lengths $L = 50\lambda$ and 200λ , respectively. Note that at such a density, reflection from the vacuum-plasma boundary is neglectable as compared to the Raman backscattered wave shown in Fig. 9 according to the well-known Fresnel formula. If $L = 50\lambda$, the backscattered wave appears with a high amplitude only in a time duration less than 100 laser cycles. Therefore, it can assist to accelerate electrons only within this time domain. Beyond this time domain, the amplitude of the corresponding backscattered wave is too low to trigger the stochastic electron motion, as illustrated by the corresponding energy distribution in Fig. 7(b). For the same plasma length but at a higher density such as $n = 0.04n_c$, the time dependence of the Raman backscattered wave appears similar to Fig. 9(a). However, its amplitude is much higher so that stochastic acceleration can sustain a long time, leading to the energy distributions given Fig. 8(a). Similarly, if $L = 200\lambda$, the high-amplitude Raman backscattered wave appears in much long time domain even if $n = 0.01n_c$. Therefore, the mechanism of stochastic accel-

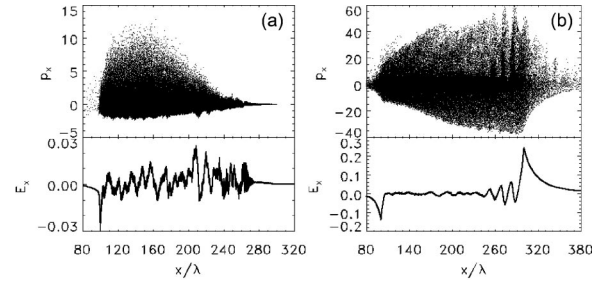


FIG. 10. Electron distributions in the longitudinal phase space found when a semi-infinite laser pulse at the peak amplitude $a_1 = 3.0$ propagates through a plasma slab, which is initially at a density $n = 0.01n_c$ and with a thickness of $L = 200\lambda$. The lower frames show the longitudinal electric field in the simulation box. (a) At $t = 300\tau$; (b) at $t = 800\tau$.

eration can work continuously, leading to the energy distributions given in Fig. 8(b).

On the other hand, Fig. 9 shows that the amplitude the Raman backscattered wave changes from period to period in a random way, i.e., it appears like a stochastic transverse field. As a result, the electron acceleration in these cases can be explained alternatively with the mechanism proposed in Ref. [15], even though the Raman backscattered wave does not appear like a white noise as adopted there. Assume there is a planar laser pulse with amplitude a_1 and a transverse stochastic field $R(t)$, where the latter is simply in a Gaussian random distribution with $\langle R \rangle = 0$ and $\langle R(t)R(t') \rangle = D\delta(t - t')$, here D the diffusion coefficient in momentum space normalized by $m^2c^2\omega_1$. Direct numerical calculation with the equation of motion in a way described in Ref. [15] shows that electrons can be accelerated up to a temperature of 12 MeV and to the maximum energy around 50 MeV within the interaction time of 150 laser cycles for the laser amplitude $a_1 = 3.0$ and $D = 0.01$. This is comparable to what is observed from PIC simulations at similar conditions. Alternatively, the acceleration process can be described by a Fokker-Planck equation [38]. Numerical calculations with this equation produce a temperature scaling for hot electrons similar to that found in Ref. [15] and in the PIC simulations as discussed later.

To see how electrons are accelerated with time, we plot electron distributions in the longitudinal phase space at different times. Figure 10 is obtained for the case when a single laser pulse propagates in a plasma slab with a length of $L = 200\lambda$. Figure 10(a) shows the snapshot when the laser pulse front propagates just through the plasma slab. Electron energy increases continuously with time and in space from the right to left up to beyond the ponderomotive potential of the laser pulse. One notes that the induced electrostatic field is at a quite low level. Therefore electron acceleration through plasma-wave excitation can be excluded. At later time, electrons are accelerated to a higher level as shown in Fig. 10(b), where electrostatic field remains to be at a low level except near the plasma-vacuum boundaries. These figures serve as an obvious evidence of direct laser acceleration. More evidences about this are given as following.

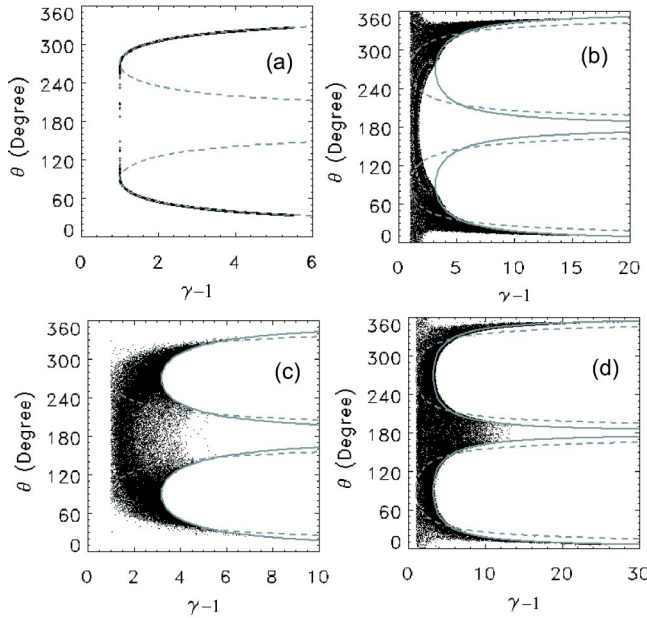


FIG. 11. Angular distributions of electrons vs the relativistic factor γ under the interaction of either a single laser pulse or two counterpropagating laser pulses. (a) With test electrons in vacuum when $a_1=3.0$ and $a_2=0.0$; (b) with test electrons in vacuum when $a_1=3.0$ and $a_2=0.1$; (c) with a plasma slab at density $n=0.01n_c$ and thickness $L=50\lambda$ when $a_1=3.0$ and $a_2=0.0$; (d) with a plasma slab at density $n=0.01n_c$ and thickness $L=50\lambda$ when $a_1=3.0$ and $a_2=0.1$. The gray solid line is for $\tan(\theta) = \pm 1/\sqrt{(\gamma^2-1)/a_1^2-1}$ and the gray dashed line is for $\tan(\theta) = \pm \sqrt{2/(\gamma-1)}$.

C. Evidences of direct laser acceleration

In the case of electron acceleration in counterpropagating laser fields, one expects that energetic electrons move predominantly along the propagating direction of the more intense one of the two pulses when $a_1 \gg a_2$, as suggested by Fig. 1. In the case of electron acceleration by a single laser pulse, there exists a well-known formula relating the energy of scattered electrons to the angle θ , which is given by [2,18]

$$\tan(\theta) = \pm [2/(\gamma-1)]^{1/2}. \quad (10)$$

Figure 11(a) shows the angular directions of electrons accelerated by a single laser pulse in vacuum, which is well described by Eq. (10). Here the forward-moving pulse propagates along $\theta=0^\circ$. In the case with two intersecting laser pulses, the angular directions of electrons are related to their kinetic energy by Eq. (4) in general. Therefore it is interesting to check if the hot electrons observed in the simulations also follow this relation. In case with counterpropagating laser fields, we have $\alpha=90^\circ$ and $C=p_{y0}$ in Eq. (4). However, in the presence of the laser fields, one should use $C=p_{y0} + (A_2 - A_1)\sin\alpha$. If $p_{y0}=0$, the value of C ranges from 0 to a_1 for $a_1 \gg a_2$. Therefore the high energy electrons basically follow

$$\tan(\theta) = \pm [(\gamma^2-1)/a_1^2-1]^{-1/2}. \quad (11)$$

For $\gamma > 1 + a_1^2/2$, this formula predicts a smaller angle along the forward direction than that predicted by Eq. (10). Figure 11(b) shows the angular directions of electrons by two counterpropagating laser pulses in vacuum. Obviously Eq. (11) agrees with the numerical simulations better than Eq. (10) does for those most energetic electrons. Figure 11(c) shows the angular direction of electrons accelerated by a single pulse in plasma. Even in this case, Eq. (11) agrees with numerical simulations better than Eq. (10) does. This in turn indicates that the stochastic acceleration with two counterpropagating pulses is responsible for the most energetic electrons in this case because of the excitation of Raman back-scattered waves. When the second counterpropagating pulse is additionally applied, the directions of high energy electrons agree with Eq. (11), as shown in Fig. 11(d). For those electrons with relatively low energy that does not follow Eq. (11), the induced electrostatic field should be a responsible factor [33].

In PIC simulations, there is another way to check whether the energetic electrons gain energy from the transverse laser fields or from the induced longitudinal fields. It is to make use of the relation $\gamma = 1 + \Gamma_{\parallel} + \Gamma_{\perp}$, following the equation of motion for electrons [13,16], where $\Gamma_{\parallel} = -\int_0^t dt' E_x v_x$ and $\Gamma_{\perp} = -\int_0^t dt' E_{\perp} v_{\perp}$, E_x and E_{\perp} are the normalized longitudinal and transverse electric fields, respectively. Here Γ_{\parallel} stands for the energy gain due to the longitudinal electric field, while Γ_{\perp} represents the contribution of direct laser acceleration by the transverse field. The energy gain from the laser field is eventually directed in the longitudinal direction through the Lorentz force. Figure 12 shows examples of electrons distributed in the $\Gamma_{\parallel} \sim \Gamma_{\perp}$ space found from both 1D and 2D PIC simulations of the interaction of two counterpropagating laser pulses with underdense plasma slabs. It demonstrates that electrons are accelerated mainly by the transverse laser fields in all these cases.

D. Two-dimensional effects

PIC simulations in 2D geometry can introduce new effects such as Raman side-scattering [31], return electron currents in the surrounding regions of the laser beam center, and new acceleration mechanism such as the betatron resonance mechanism [16]. As a result, it is expected that electrons can be accelerated to a different level from the 1D simulations for the fixed laser pulse and plasma parameters. To check how stochastic acceleration works in the 2D geometry, we conduct a series of 2D PIC simulations. Snapshots of the obtained energy distributions are given in Fig. 13. In the 2D geometry, there are two different cases for the incident laser pulses, i.e., they are P polarized if the electric field components are within the simulation plane or S polarized if the electric field components are perpendicular to the simulation plane. Figure 13(a) shows the energy distributions either with or without the second counterpropagating pulse for the P polarization case. As the same as that found in 1D PIC simulations, with the presence of the counterpropagating pulse, electrons are accelerated to much high level than without it. Figure 13(b) displays the energy distributions for the S -polarization case. It is obvious that the mechanism of sto-

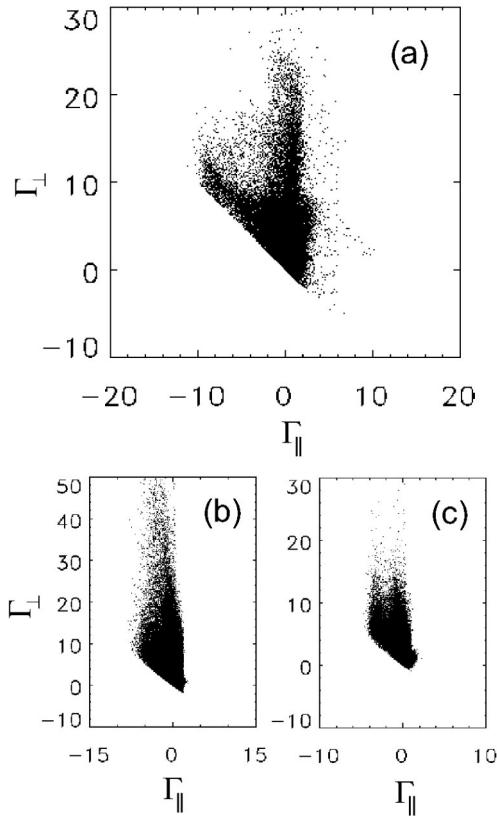


FIG. 12. Electron energy gain from longitudinal fields vs that from transverse laser fields when the two counterpropagating laser pulses interact with a plasma slab at density $n=0.01n_c$ and thickness $L=50\lambda$. (a) From a 1D PIC simulation for $a_1=3.0$ and $a_2=0.1$ at $t=300\tau$; (b) from 2D PIC simulation for $a_1=3.0$ and $a_2=0.2$ at $t=160\tau$ when the incident pulses are P polarized; (c) from 2D PIC simulation for $a_1=3.0$ and $a_2=0.2$ at $t=160\tau$ when the incident pulses are S polarized.

chastic heating and acceleration also works in this case. Furthermore, in the presence of the second counterpropagating laser pulse, it appears that electron acceleration in the P -polarization case is more efficient than in the S -polarization case. This can be partially attributed to set-in of the betatron resonance mechanism [16] in P polarization, which is absent in S polarization. However, one also notes that, without the presence of the counterpropagating pulse, electrons are accelerated to a similar low level for the two polarization cases.

Corresponding to the electron energy distributions, the quasistatic current and magnetic field in the presence of the second pulse are found to be significantly increased than that without it. As shown in Figs. 14(a) and 14(b), the peak quasistatic magnetic field in the case with the second counterpropagating pulse (even though at an amplitude $a_2=0.1$) is more than three times larger than that without it. We note that the maximum quasistatic currents and magnetic fields found for the two polarization cases are comparable, even though the maximum electron energy found for the P -polarization case is much higher than for the S -polarization case when the counterpropagating laser pulse is applied.

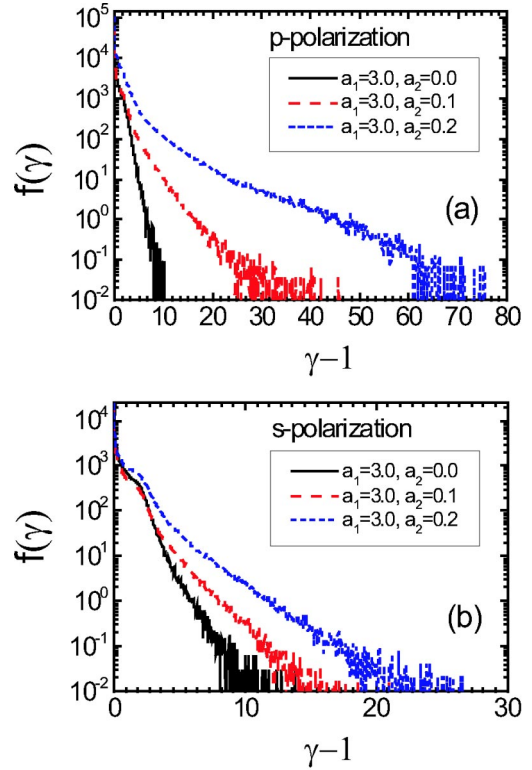


FIG. 13. Snapshots of electron energy distributions (not normalized) from 2D PIC simulations of laser interaction with a plasma slab at density $n=0.01n_c$ and thickness $L=50\lambda$ at $t=140\tau$. (a) For the P polarization; (b) for the S polarization. The laser pulses are semi-infinite.

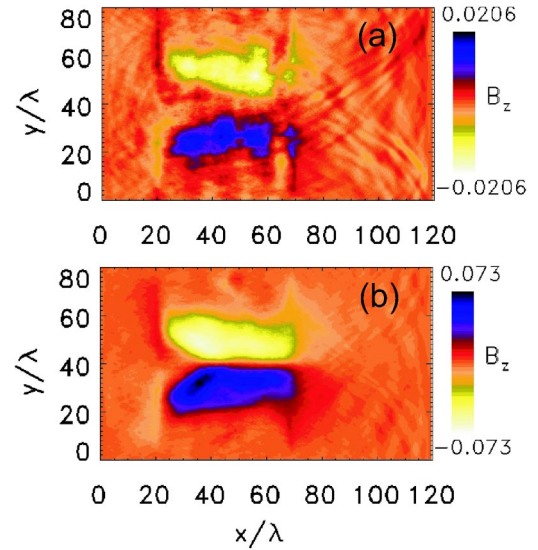


FIG. 14. (Color online). Quasistatic magnetic fields from 2D PIC simulations of laser interaction with a plasma slab at density $n=0.01n_c$ and thickness $L=50\lambda$ at $t=160\tau$. Both the laser pulses are S polarized and semi-infinite. (a) $a_1=3.0$ and $a_2=0.0$; (b) $a_1=3.0$ and $a_2=0.2$.

E. Electron energy scaling

To see the dependence of electron temperatures on the pulse amplitudes, we take a plasma slab with a thickness of $L=50\lambda$ and at a low density $n=0.01n_c$ to avoid the high Raman backscattered wave. A series of 1D PIC simulations have been conducted by changing either a_1 or a_2 . For the interested forward acceleration rather than the isotropic heating, we usually take $a_1 \gg a_2$. Through these simulations, it is found that, at early time well before the hot electron heating gets saturated, the hot electron temperature and the maximum electron energy scale proportional to $\sim a_1^{\delta_1} a_2^{\delta_2} t^{\delta_3}$, where t is the interacting time duration, δ_1 , δ_2 , and δ_3 are factors related to pulse profile and amplitudes. For the case with semi-infinite laser pulses, we have roughly $\delta_1 \sim 2$ and $\delta_2 \sim 0.5$; while for pulses with finite pulse durations, we have roughly $\delta_1 \sim 1$ and $\delta_2 \sim 0.5$ after the laser pulses pass through the plasma region. These two different scaling laws with the intensity of the first pulse can be associated with different ponderomotive pushes in these two cases. With pulses with finite durations, electrons experience not only an initial forward ponderomotive push at the leading edge but also a corresponding opposite push from the pulse tail, where the latter reduces the final energy gain. Scaling to the time duration is normally like $\delta_3 \approx 0.5-1.0$. This scaling agrees qualitatively to what we found before for electron acceleration by an intense laser pulse in the presence of a stochastic field [15,38], where it is found that the hot electron temperature scales proportional to the square root of laser intensity and depends relatively weakly upon the level of the stochastic field. Finally, for an intense pulse with a finite but sufficiently long duration such as a few hundred laser cycles, even if the opposite ponderomotive push from the pulse tail may obviously change the electron energy spectrum around the ponderomotive potential level, it cannot change the energy spectrum significantly at the regime with a much higher energy level.

IV. SUMMARY

In summary, we propose a scheme that can efficiently accelerate electrons to a temperature much higher than the laser ponderomotive potential by use of two counterpropagating laser pulses either in vacuum or in underdense plasma. The acceleration is triggered as soon as stochastic motion of electrons occurs. The threshold amplitudes for the stochastic motion have been found numerically. It is found that the preacceleration of electrons by the ponderomotive force of a forward-propagating laser pulse can largely reduce the threshold amplitude of the counterpropagating pulse for

triggering the stochastic motion. Particle-in-cell simulations show that this mechanism can be dominant in laser interaction with underdense plasma, where the counterpropagating wave could either be the Raman backscattered/side-scattered wave of an incident pulse in underdense plasma or the reflected wave of the pulse from overdense plasma regions. Energetic electrons generated through this scheme move predominantly in the propagation direction of the pulse with relatively higher intensities. In addition, the Raman backscattered/side-scattered wave of a high intensity laser pulse can also serve as a stochastic field, which dephases electrons and thereby allows for net energy transfer from the laser to electrons as suggested in Ref. [15].

In the interaction of subpicosecond intense laser pulses with plasmas at moderate densities such as a few tens percent of the critical density, the present acceleration mechanism may play a dominant role for observed particle acceleration. In this circumstance, it can be more efficient than the well-known mechanism of self-modulated laser wake-field acceleration (SM-LWFA), because electron acceleration by a plasma wave is limited by its phase velocity. The SW-LWFA is efficient only in tenuous plasma, where the phase velocity of the generated plasma wave is so high as very close to the vacuum speed of light. In plasmas at moderate densities, however, the Raman backscattering can be easily excited to a high level and trigger the stochastic acceleration of electrons. For relativistic-intense laser pulses, the Raman backscattered and side-scattered waves of the incident laser pulses can be excited even if the plasma density is larger than $n = 0.25n_c$. This is partially owing to the relativistic effect and partially owing to the merging of the Raman scattering instability with the relativistic modulation instability in the wave-vector space [22,34-37]. As a result, the stochastic heating and acceleration of electrons should occur throughout all underdense plasma regions where the intense laser pulse can propagate.

ACKNOWLEDGMENTS

We acknowledge stimulating discussions with Y. Sentoku, M. Jovanovic, T. Taguchi, and D. Umstadter on this work. This work was supported in part by the National Natural Science Foundation of China (Grant Nos. 10105014, 19825110, and 10075075), the National High-Tech ICF Committee of China, the National Key Basic Research Special Foundation (Grant No. G1999075200), the Japan-China Core University program, and the Bundesministerium für Bildung und Forschung (BMBF) and the Deutsche Forschungsgemeinschaft of Germany.

-
- [1] G.A. Mourou, C.P.J. Barty, and M.D. Perry, *Phys. Today* **51(1)**, 22 (1998); G. Mourou and D. Umstadter, *Sci. Am.* **81** (May, 2002).
 [2] J. Meyer-ter-Vehn, A. Pukhov, and Z.-M. Sheng, in *Atoms, Solids, and Plasmas in Super-Intense Laser Fields*, edited by D. Batani *et al.* (Kluwer Academic/Plenum, New York, 2001),

pp. 167-192.

- [3] D. Umstadter, *Phys. Plasmas* **8**, 1774 (2001).
 [4] M. Tabak *et al.*, *Phys. Plasmas* **1**, 1626 (1994).
 [5] J. Meyer-ter-Vehn, *Plasma Phys. Controlled Fusion* **43**, A113 (2001).
 [6] A. Pukhov, *Phys. Rev. Lett.* **86**, 3526 (2001); Y. Sentoku *et al.*,

- Appl. Phys. B: Lasers Opt. **74**, 207 (2002); S.C. Wilks *et al.*, Phys. Plasmas **8**, 542 (2001); A.J. Mackinnon *et al.*, Phys. Rev. Lett. **88**, 215006 (2002); Z.Th. Esirkepov *et al.*, *ibid.* **89**, 175003 (2002).
- [7] P. Norryes, Phys. Plasmas **6**, 2150 (1999).
- [8] C. Gahn *et al.*, Appl. Phys. Lett. **73**, 3662 (1998).
- [9] M.N. Rosenbluth and C.S. Liu, Phys. Rev. Lett. **29**, 701 (1972); T. Tajima and J.M. Dawson, *ibid.* **43**, 267 (1979).
- [10] E. Esarey, P. Sprangle, J. Krall, and A. Ting, IEEE Trans. Plasma Sci. **PS-24**, 252 (1996).
- [11] V. Malka *et al.*, Science **298**, 1596 (2002).
- [12] D. Umstadter *et al.*, Phys. Rev. Lett. **76**, 2073 (1996); E. Esarey *et al.*, *ibid.* **79**, 2682 (1997).
- [13] Z.-M. Sheng, K. Mima, Y. Sentoku, K. Nishihara, and J. Zhang, Phys. Plasmas **9**, 3147 (2002).
- [14] G.R. Smith and A.N. Kaufman, Phys. Rev. Lett. **34**, 1613 (1975); Phys. Fluids **21**, 2230 (1978); C.R. Menyuk *et al.*, Phys. Rev. Lett. **58**, 2071 (1987); S. Kawata, *ibid.* **66**, 2072 (1991); M.S. Hussein and M.P. Pato, *ibid.* **68**, 1136 (1992); Y. Gell and R. Nakach, Phys. Rev. E **55**, 5915 (1997).
- [15] J. Meyer-ter-Vehn and Z.M. Sheng, Phys. Plasmas **6**, 641 (1999).
- [16] A. Pukhov, Z.-M. Sheng, and J. Meyer-ter-Vehn, Phys. Plasmas **6**, 2847 (1999); C. Gahn *et al.*, Phys. Rev. Lett. **83**, 4772 (1999).
- [17] Z.-M. Sheng, K. Mima, Y. Sentoku, M. Jovanovic, T. Taguchi, J. Zhang, and J. Meyer-ter-Vehn, Phys. Rev. Lett. **88**, 055004 (2002).
- [18] G. Schmidt and T. Wilcox, Phys. Rev. Lett. **31**, 1380 (1973); C.I. Moore *et al.*, *ibid.* **74**, 2439 (1995); F.V. Hartmann *et al.*, Phys. Rev. E **51**, 4833 (1995); B. Rau *et al.*, Phys. Rev. Lett. **78**, 3310 (1997); E. Esarey *et al.*, Phys. Rev. E **52**, 5443 (1995); C.J. McKinstrie and E.A. Startsev, *ibid.* **56**, 2130 (1997); B. Quesnel and P. Mora, *ibid.* **58**, 3719 (1998).
- [19] F. Brunel, Phys. Rev. Lett. **59**, 52 (1987).
- [20] W.L. Kruer and K. Estabrook, Phys. Fluids **28**, 430 (1985).
- [21] G. Shvets *et al.*, Phys. Rev. E **60**, 2218 (1999); Phys. Plasmas **9**, 2383 (2002).
- [22] J.C. Adam *et al.*, Phys. Rev. Lett. **78**, 4765 (1997).
- [23] Y. Sentoku *et al.*, Appl. Phys. B: Lasers Opt. **74**, 207 (2002).
- [24] K.-C. Tzeng, W.B. Mori, and T. Katsouleas, Phys. Rev. Lett. **79**, 5258 (1997).
- [25] P. Zhang, N. Saleh, C. Chen, Z.M. Sheng, and D. Umstadter, Phys. Plasmas **10**, 2093 (2003); Phys. Rev. Lett. **91**, 225001 (2003).
- [26] E.S. Sarachik and G.T. Schappert, Phys. Rev. D **1**, 2738 (1970).
- [27] G.M. Zaslavskii and N.N. Filonenko, Sov. Phys. JETP **25**, 851 (1968); A.B. Rechester and T.H. Stix, Phys. Rev. A **19**, 1656 (1979); D.F. Escande and F. Doveil, Phys. Lett. A **83**, 307 (1981); **84**, 399 (1981).
- [28] D. Bauer, P. Mulse, and W.H. Steeb, Phys. Rev. Lett. **75**, 4622 (1995); G. Schmidt, Comments Plasma Phys. Controlled Fusion **7**, 87 (1982).
- [29] J.T. Mendonca and F. Doveil, J. Plasma Phys. **28**, 485 (1982); Phys. Rev. A **28**, 3592 (1983).
- [30] A.J. Lichtenberg and M.A. Lieberman, *Regular and Stochastic Motion* (Springer-Verlag, New York, 1981), and references therein.
- [31] D.W. Forslund *et al.*, Phys. Rev. Lett. **54**, 558 (1985).
- [32] B.V. Chirikov, Phys. Rep. **52**, 263 (1979).
- [33] Z.-M. Sheng *et al.*, Phys. Rev. Lett. **85**, 5340 (2000); Z.-M. Sheng and J. Meyer-ter-Vehn, in *Superstrong Fields in Plasmas*, edited by M. Lontano, G. Mourou, F. Pegarars, and E. Sindoni, AIP Conf. Proc. **426** (AIP, Woodbury, 1998), 153.
- [34] Z.-M. Sheng, K. Mima, Y. Sentoku, and K. Nishihara, Phys. Rev. E **61**, 4362 (2000).
- [35] K. Mima, M. Jovanovic, Y. Sentoku, Z.M. Sheng, M. Skoric, and T. Sato, Phys. Plasmas **8**, 2349 (2001).
- [36] B. Quesnel, P. Mora, J.C. Adam, A. Heron, and A. Laval, Phys. Plasmas **4**, 3358 (1997).
- [37] S. Guerin, A. Laval, P. Mora, J.C. Adam, and A. Heron, Phys. Plasmas **2**, 2807 (1995).
- [38] T. Nakamura, S. Kato, M. Tamimoto, and T. Kato, Phys. Plasmas **9**, 1801 (2002).